Lidar methods for remote sensing of pollution in the upper ocean layer

V.G. Bondur and E.V. Zubkov

Central Scientific Research Institute "Kometa," Moscow

Received January 3, 2001

Lidar methods for remotely sensing pollution of the marine environment and physical effects they are based on are discussed. These methods are promising for monitoring of the upper ocean layer because of their capability of monitoring the fields of a wide variety of different properties (physical, chemical, and biological). The efficiency of the proposed lidar methods is confirmed by field and laboratory experiments, as well as by theoretical studies.

Introduction

Remote monitoring of pollution of the World Ocean becomes especially important nowadays, and lidar methods occupy a significant place among the methods of remote monitoring.[1–10] Various types of anthropogenic impact on the water medium change its parameters, and the most part of these changes can be detected with lidars. The main advantage of the lidar methods as compared to other remote methods is the capability of studying a wide range of characteristics of the water medium in combination with such their advantages as the possibility of nondestructive control, short measurement time (practically, no delay), high depth resolution (with the corresponding power characteristics of a lidar), high productivity, possibility of real-time or nearly real-time operation.

The above-listed advantages of the lidar methods are invaluable when monitoring the anthropogenic impact on the ocean ecosystems and predicting changes of the ecosystems under the effect of various factors. This is especially important in the development of systems for environmental monitoring.[8–13]

This paper considers the lidar methods for sensing the upper ocean layer that are especially efficient for remotely monitoring pollution of seas and oceans.

1. Physical principles of lidar methods

The lidar methods for monitoring of different properties of water media are mostly based on the effects of elastic and inelastic interaction of radiation with the matter.[1–7,14–18] The use of these effects in combination with other physical effects inherent in electromagnetic radiation (interference, polarization, Doppler effect, etc.) along with the application of spectroscopic methods explains the variety of the lidar methods of monitoring of the water medium.[1–5,18,19]

In the case of elastic interaction, Rayleigh scattering (by water molecules) and Mie scattering (on suspended particles) take place. The information on characteristics of the sea medium is contained in the amplitude-time structure of a backscattered signal at an unshifted wavelength of sounding radiation.

Examples of inelastic interactions are spontaneous Raman scattering, fluorescence, stimulated Brillouin scattering (SBS), and others. A lot of information contained in spectra of the secondary emission allows one to solve many problems associated with diagnostics of pollution of the water medium, but the basic power characteristic of these processes – backscattering cross section – is several orders of magnitude lower than that for the elastic interaction. This limits the applicability of the methods based on the effects of inelastic interactions because of the limited resolution and the depth range for realistically achievable power characteristics of the airborne lidars.

Combined methods based on a combination of the effects of elastic and inelastic interactions are also known. A characteristic example is a method of normalization of signals (Mie scattering, fluorescence) or partial components of their spectra to the Raman scattering signal.[5,20]

The lidar methods of sensing the marine environment are directly connected with the complicated solution of the inverse problems of laser hydrooptics, which are aimed at determining that or other hydrophysical characteristics in a given elementary volume of the marine medium from the response to a sounding pulse. Solution of the inverse problems is complicated because of the presence of numerous random factors distorting the amplitude-time structure of signals. The main difficulties are connected with the influence of a rough sea surface on the propagation of a collimated laser beam and the presence of natural random inhomogeneities in the hydrophysical properties of the marine medium.

The methods for solution of the inverse problems of laser sensing are based on the equation of radiative transfer in an inhomogeneous absorbing and scattering medium.[14–16,21] This equation, with the allowance made for a lot of assumptions on the characteristics of the sounding radiation, propagation media and their interface, specificity of lidar operation and actual instrumental characteristics of lidars, as well as assumptions on the space-time distribution of the primary hydrooptical characteristics of a specific type of the marine medium, is reduced, as a rule, to the lidar

0235-6880/01/02 128-13 $02.00

equation in the small-angle approximation of single scattering.[2,14] The equation given below is valid for the case of sensing through a smooth interface from the height H

$$U(L) = A\, P_0\, \frac{c\tau_p}{2n}\, [\tau_a(1-\rho)]^2 \times$$

$$\times \frac{\sigma(\pi, L)}{(H + L/n)^2} \exp\left[-2\int_0^L \varepsilon(l)\, dl\right], \qquad (1)$$

where U is the signal amplitude; L is the depth; A is the lidar instrumental constant; P_0 is the laser pulse power; c is the speed of light; τ_p is the duration of a sounding pulse; $\tau_a = \int_0^H \varepsilon_a(l)\, dl$ is the atmospheric transmission coefficient, ε_a is the extinction coefficient of the atmosphere; ρ is the Fresnel reflection index of the sea surface; $\varepsilon = \sigma + \chi$ is the extinction coefficient of the marine medium, σ is the scattering coefficient (integral over the full solid angle value); χ is the absorption coefficient; $\sigma(\pi, L)$ is the backscattering coefficient; n is the refractive index of the sea water.

This equation for the case of Mie scattering written with the allowance for the accepted assumptions has some modifications connected with different cross sections of the physical effects (spontaneous Raman scattering, fluorescence, etc.) forming the basis for the sensing methods.[2–5] In this paper, the methods and results of lidar studies are considered, as a rule, based on the equation of a monostatic lidar in the small-angle approximation of single scattering. Now this corresponds to the actual situation for the overwhelming majority of lidars, although the interest that has been shown in recent years to deep sensing lidars with a wide beam should also be mentioned.[22]

The below table classifies the laser sensing methods, which can be used for determining various characteristics of the upper ocean layer.

This table of course is not complete: in particular, it does not include methods employing the Doppler effect, as well as methods of laser sensing of the sea surface. In some cases, we mention the methods that are not still beyond the framework of laboratory experiments, but are rather promising, in our opinion (for example, methods of correlation and nonlinear spectroscopy[5,23–25]).

Below we consider physical effects that form the basis for the lidar methods presented in the table.

2. Methods based on elastic interaction of laser radiation with matter

Application of such methods is based on analysis of an envelope of the backscattering pulse at an unshifted wavelength of laser radiation corresponding to minimum extinction in the region of a "transparency window" of the marine medium.[14,26] As known, the contribution of the Rayleigh scattering even in most transparent waters does not exceed ~ 10% (Ref. 14). Therefore, the decisive factor in formation of the envelope of the backscattered signal is Mie scattering on suspended particles, whose size is comparable with the wavelength of sounding radiation.

Table. Laser methods for studying pollution of sea medium

Type of interaction of radiation with matter	Physical effects and methods based on them		Studied characteristics and monitored parameters									
			Hydrodynamic perturbations	Turbidity	Phytoplankton	Chlorophyll	DOM	OP	Bacterial component	Heavy metals	Temperature (T)	Salinity (S)
			Set of indices of spatio-temporal variability	Relative values: $\sigma(L)$* – scattering $\varepsilon(L)$ – extinction	Composition (identification of components). Concentration						$T(L)$	$S(L)$
Elastic		Methods of inversion of lidar equation	■	■	■							
		Method of local gradient extrema	■	■	■							
		Two-channel polarization method	■	■								
	Methods of linear spectroscopy											
	Interference. Formation of dynamic biospeckles	Correlation spectroscopy							■			

Table (continued)

Type of interaction of radiation with matter	Physical effects and methods based on them		Studied characteristics and monitored parameters									
			Hydrodynamic perturbations	Turbidity	Phytoplankton	Chlorophyll	DOM	OP	Bacterial component	Heavy metals	Temperature (T)	Salinity (S)
			Set of indices of spatio-temporal variability	Relative values: $\sigma(L)$* – scattering $\varepsilon(L)$ – extinction	Composition (identification of components). Concentration						$T(L)$	$S(L)$
Combined methods of elastic and inelastic interactions	Mie scattering and spontaneous Raman scattering	Method of normalization to Raman scattering signal										
	Fluorescence and spontaneous Raman scattering											
Inelastic	Spontaneous Raman scattering	Change in ratio of spectral components of monomer and polymer phases of water										
		Polarization										
		Analysis of spectrum envelope										
		Measurement of integral parameter of fluorescence			Mapping of fluorescence field							
		Analysis of fluorescence spectrum										
		Nonlinear fluorimetry										
		Multifrequency fluorimetry										
		Method of 3D matrices										
		Multispectral fluorimetry										
	Methods of nonlinear spectrometry											
	Coherent Raman scattering	CARS (coherent anti-Stokes Raman scattering)										
		KOR (Kerr optical resonance)										
	Stimulated Brillouin scattering	SBS method										
	Plasma breakdown	Laser-spark method										

*L is depth; – experimentally approved data; – theoretical studies and laboratory experiments.

The turbidity field is analyzed as a generalized characteristic of pollution of the marine medium with the use of Eq. (1). The amplitude-time structure of the backscattering signal bears the information on the spatial distribution and concentration of a suspension (via the values of σ and $\sigma(\pi)$), on the presence of various chemical compounds and elements dissolved in the sea water (via the value of χ), and on the presence of temperature inhomogeneities, including those due to turbulence (via the value of n).

The values of χ or σ can be estimated separately from Eq. (1) based on certain assumptions concerning the specific type of the sea water, depth range, and spatial and geometric characteristics of the receiving and transmitting systems of a lidar. In other words, that or other physical model of sensing of the marine medium, on the corresponding assumptions about the primary hydrooptical characteristics, leads to the approximation of the radiative transfer equation and determines finally the requirements to lidar characteristics.[2,3,15]

For example, when studying the upper ocean layer along an optical path with $\tau < 15 - 20$ ($L < 100$ m) in the case that multiple scattering processes do not prevail at the wavelength corresponding to the transparency window (no asymptotic conditions) for water, in which the variability of χ with depth is markedly less than the variability of σ, the amplitude–time structure of the backscattered signal is primarily determined by the integral parameter σ and the scattering phase function $\sigma(\pi)$ in a small solid angle about the backward direction that depends on lidar geometry.[14] In general, the value of $\sigma(\pi)$, in view of some physical reasons, is ambiguously connected with the integral parameter σ (in the complete solid angle). In this case, as follows from Eq. (1), the small-structure time variability is mostly determined by the backscatter value.

The existing lidar methods for diagnostics of the turbidity field are mostly based on estimation of space-time variability of signal characteristics not related to absolute values of the primary hydrooptical characteristics.

2.1. Method of inversion of the lidar equation

A stable form of inversion of the lidar equation is known.[27] The inversion here means solving the inverse problem, namely, reconstruction of the vertical depth profile $\varepsilon(L)$ from the envelope of the return signal $U(L)$. This form

$$\varepsilon(r) = \frac{\exp\left[\dfrac{S(r) - S_m}{k}\right]}{\dfrac{1}{k} + \dfrac{2}{k}\displaystyle\int_r^{r_m} \exp\left[\frac{S(r') - S_m}{k}\right] dr'}, \qquad (2)$$

was applied to return signals in both the atmosphere[27,28] and the water medium.[7,29] Here $S(r) = \ln [P(r)\, r^2]$ is the logarithm of range-weighted power $P(r)$ of the return signal; r is the range; r' is the current value of the range; r_m is the maximum distance along the sounding path; $S_m = S(r_m)$.

The solution is obtained assumed that there exists the dependence $\sigma = B\, \varepsilon^k$, where B and k are constants, and k varies from 0.67 to 1.0 depending on the type of scattering particles. However, although this solution is stable to signal fluctuations especially significant within a finite section of a sounding path at low power of the return signal, it does not take into account the effects of multiple scattering.

The modified form of the solution with a correction made for variation of the beam cross section in an inhomogeneous scattering medium (in the small-angle approximation) was obtained in Ref. 31 in accordance with Ref. 30

$$\varepsilon(r) = \frac{\left[\dfrac{F(r)}{F(r_m)}\right]^{1/k} \exp\left[\dfrac{S(r) - S_m}{k}\right]}{\dfrac{1}{\varepsilon_m} + \dfrac{2}{k}\displaystyle\int_r^{r_m} \left[\frac{F(r')}{F(r_m)}\right]^{1/k} \exp\left[\frac{S(r') - S_m}{k}\right] dr'}, \qquad (3)$$

where

$$F(r) = 1 + \left(\frac{\nu}{nH + r}\right)^2 \int_0^r \sigma(\xi)\, (r - \xi)^2\, d\xi; \qquad (4)$$

$\nu = \gamma_0\, n/\tan\alpha$; $\gamma_0^2(\xi)$ is the variance of the angle of deflection at a single scattering event; α is the angular divergence of the laser beam; $\varepsilon_m = \varepsilon(r_m)$.

The results on relative values of $\varepsilon(r)$ reconstructed by solving Eq. (3) showed a significant decrease of the errors especially for the cases of stratification with a pronounced maximum (up to 2 to 3 times at the maximum point). In the numerical simulations, various simple functional dependences were used for $\varepsilon(r)$. Since in the actual situation the profile $\varepsilon(r)$ is *a priori* unknown, the functional (4) for the case of a homogeneous medium ($\sigma(r) = \text{const}$) was used for reconstruction. It turned out that this does not lead to marked errors. So, this algorithm can be applied to processing actual signals. For calibration of the scale of ε in absolute values, synchronous contact measurements are needed. This, in turn, is connected with a technically difficult problem of mutual calibration of remote and contact instruments.

2.2. Method of local extrema of the return signal gradient

Acquiring information on the structure and characteristics of the marine medium from analysis of the envelope of the Mie backscatter is complicated by the problem of data interpretation. This is connected with the fact that the envelope of the backscattering signal is not adequate to variations of hydrooptical characteristics because of the effects of multiple scattering and roughness of the sea surface on propagation of a collimated laser beam and the return signal, as well as because of the strongly nonlinear

behavior of radiation extinction with distance. In this case, the variance of the return signal amplitude is significant and besides, it is increased even more due to the action of a number of other factors accompanying operation of an airborne lidar (vibration and random perturbations of the aircraft position when flying in the turbulent atmosphere, background illumination, influence of the near-surface atmospheric layer, etc.).

Based on the heuristic approach to a particular case of solution of the inverse problem of laser hydrooptics, the method of local gradient extrema (LGE) has been developed. This method is quite efficient for solving the problems on studying the anthropogenic impact on the marine environment.[8,12,32,33] The method deals with the characteristics of relative variability of the signal – approaching the gradients normalized to the initial amplitude of the digitized backscattering signal

$$\nabla U(k) = \frac{U(k+1) - U(k)}{U(k-1)} \cdot 100\%, \qquad (5)$$

where k is the number of the time channel in the time (depth) scale.

The depth resolution of the lidar

$$\Delta L = c\,\tau_p/2n. \qquad (6)$$

corresponds here to the time scale.

The procedure is similar to the widely used approach of revealing hidden singularities in experimental dependences, in which derivatives are used in spite of a function itself (this approach is often used, for example, in laser spectroscopy[16]). The result of its application to the digitized backscattering signal is an array of alternating-sign values of gradients (including zero values).

The LGE method consists in a logical procedure of selection of local extrema from the obtained array $\nabla U(k)$, $k = 1, \ldots, K$. This procedure is repeated for every pulse in the sample M ($m = 1, \ldots, M$). Physically, this is equivalent to selection of points with maximum rates of variation of hydrooptical characteristics in the vertical cross section of the marine medium. It seems rather logical to assume that the points of local extrema correspond to the boundaries of sublayers in the fine structure of scattering layers, in particular, in the region of seasonal thermocline.

The two-dimensional arrays of the values of local gradient extrema $[\nabla U(k, m)]_{\max}$ and $[\nabla U(k, m)]_{\min}$ separated in the analyzed sample of M pulses can be averaged both over the number μ_m of extrema in all K time channels of the mth pulse (7) and over the number μ_k of extrema in the kth time channel for all M pulses of the analyzed sample

$$\langle \nabla U(m) \rangle_{\max,\min} = \frac{1}{\mu_m} \left[\sum_{k=1}^{K} \nabla U_m(k) \right]_{\max,\min}, \qquad (7)$$

$$\langle \nabla U(k) \rangle_{\max,\min} = \frac{1}{\mu_k} \left[\sum_{m=1}^{M} \nabla U_k(m) \right]_{\max,\min}. \qquad (8)$$

The arrays of gradients with different sign are analyzed separately. Physically, the sign characterizes the variability of properties of the marine medium – increase or decrease of turbidity. This is important for monitoring of pollution.

In the proposed methods, we can also use such procedures as two-dimensional smoothing of an array over k and m, drawing of histograms of distribution of depth intervals over LGE points in a single sensing pulse, etc.

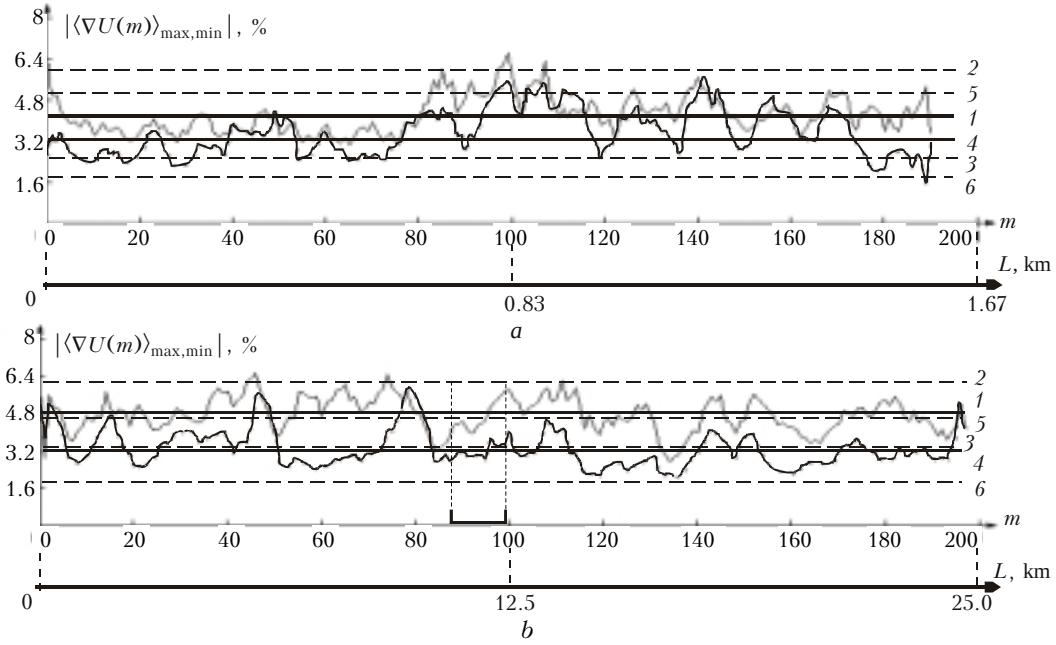

Fig. 1. Characteristics of the variability of the turbidity field. Distributions of the pulse-average values of local gradient extrema: along a path section (*a*) and a complete path (*b*); ⌊⌋ indicates the position of the section (*a*) —— $|\langle \nabla U(m)_{\min} \rangle| = E$; —— $|\langle \nabla U(m)_{\max} \rangle| = E$ are the levels of mathematical expectation of E for these realizations; levels of E for max and min, respectively, (*1* and *4*), levels of $E + \sigma$ for max and min, respectively, (*2* and *5*), and levels of $E - \sigma$ for max and min, respectively, (*3* and *6*).

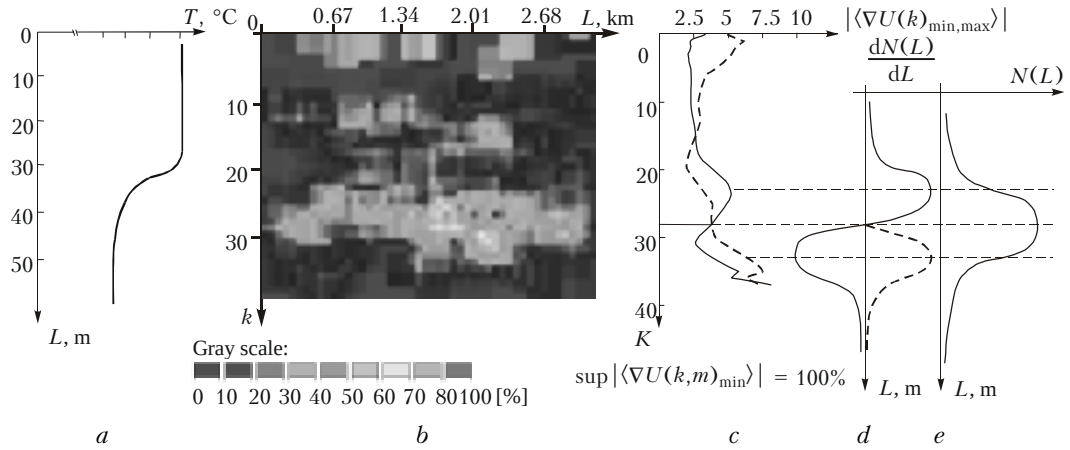

Fig. 2. Comparison of data of contact and remote measurements of depth variability of the turbidity field: contact measurements of temperature profile (in relative units) (*a*), two-dimensional distribution of local gradient extrema $|\langle\nabla U(k,m)_{\min}\rangle|$ (*b*), depth distributions (*c*): – – – $|\langle\nabla U(k)_{\min}\rangle|$ and ——— $|\langle\nabla U(k)_{\max}\rangle|$, gradient model of the scattering layer (*d*): ——— $dN(L)/dL$ and – – – $|dN(L)/dL|$, idealized model of distribution of scatterers (*e*): $N(L)$.

The efficiency of the proposed method has been confirmed in field experiments. Below we present the data obtained in filed experiments with airborne lidars in the northwestern part of the Pacific Ocean near Kamchatka. The lidar had the following characteristics: a solid-state Nd^{3+}YAG laser operated at the second harmonic ($\lambda = 532$ nm), pulse energy up to 150 mJ, pulse length of 10 ns, pulse repetition frequency of 10 Hz, angular divergence of the laser beam of $(0.5–4)\cdot10^{-3}$ rad, the entrance aperture of the receiving telescope is 280 mm, field of view of $5\cdot10^{-3}$ rad. A photomultiplier tube with a two-stage temporal regulation of amplification for compressing the dynamic range of the return signal was used as a photodetector.

Equations (7) and (8) were used for processing the experimental data. They gave an estimate for the variability of the turbidity field along the sounding direction as an average both over a layer [Eq. (7)] (Fig. 1) and over the depth [Eq. (8)] (Fig. 2) for the path section analyzed.

As follows from Figs. 2*a–c*, the position of the maximum in the scattering layer is close to the depth of the thermocline as judged from the data of contact measurements.[8] The obtained data agree with the gradient model of the scattering layer.[33] The two-dimensional smoothing of the LGE distributions in the vertical cross section of the marine medium allows revealing the structure of the scattering layer.

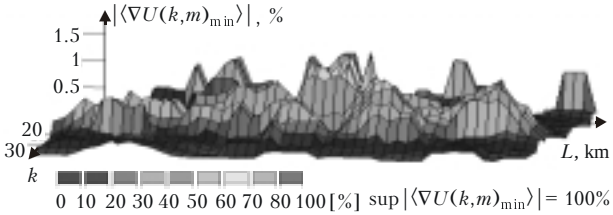

Fig. 3. 3D projection of the distribution of negative (anomalous) local gradient extrema in the vertical cross section of the marine medium.

Figure 3 shows a 3D projection of the distribution of negative (anomalous) gradient extrema in the vertical cross section of the marine medium. The smoothed LGE values are shown in the gray scale covering the entire dynamic range of the values.

Other results on revealing scattering layers by lidar methods are known as well.[34–37] Thus, Refs. 35 and 36 describe the experiments on synchronous acoustic and lidar sensing of the upper ocean layer. In these experiments, two versions of sensing were used: through the sea surface and through a dipping illuminator. For reconstruction of the profile $\varepsilon(L)$, the simplest inversion algorithm in the single-scattering approximation was used

$$\varepsilon(L) = c^{-1}\,(L_2 - L_1)^{-1}\,[\log P(L_1) - \log (P(L_2)]. \quad (9)$$

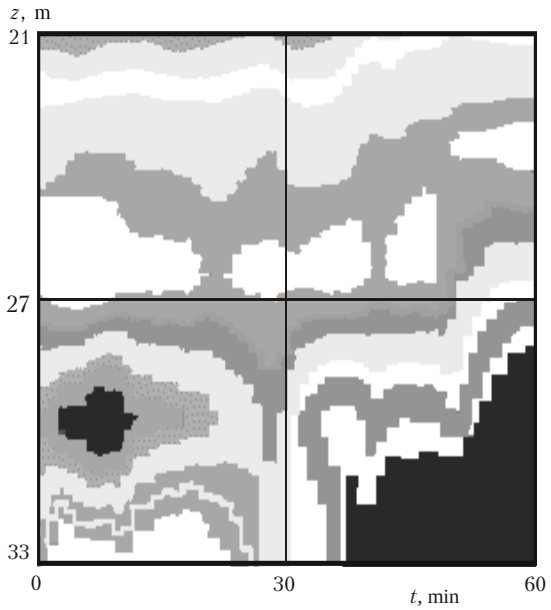

Fig. 4. Space-time field of scattering layers: cells with enhanced (▭) and low (▬) values of the extinction coefficient.

The distribution of ε in the vertical cross section of the marine medium is shown in Fig. 4. The depth range is from 21 to 33 m; this corresponds to the thermocline position. The depth resolution is 1 m. Along with the layers, cells (lenses) with enhanced values of turbidity and transparency are seen in the vertical cross section of the field of ε (Ref. 36). Similar results have been obtained by the LGE method (see Fig. 3), but on a different spatial scale.

In Ref. 37, the scattering layers were separated out by subtracting the averaged reference signal corresponding to clean, nonturbid waters from the backscattering signals received from turbid water in the shelf zone.

2.3. Method of studying the turbidity field using the effect of radiation polarization

Inhomogeneities in the vertical distribution of the suspended matter affect polarization of backscattered radiation. References 2, 34, and 38–41 consider the method of determining the vertical profile of turbidity from the time variability of the ratio of orthogonal polarization components of the backscattering signal ($F_{\|}$ $F_{\perp}$) at the initial linear polarization of the sounding signal

$$p(t) = \frac{F^{\|}(t) - F^{\perp}(t)}{F^{\|}(t) + F^{\perp}(t)}, \qquad (10)$$

where $p(t)$ is the degree of polarization.

In the small-angle approximation and assuming that the depth distribution of the scattering coefficient is proportional to the time derivative of the degree of polarization of the backscattering signal

$$\sigma(t) = -\frac{1}{c\,\Delta\alpha}\frac{\mathrm{d}}{\mathrm{d}t}[\ln p(t)], \qquad (11)$$

where $\Delta\alpha$ is the normalizing parameter, the profile $\sigma[L]$ ($L = ct/2n$) has been determined from measurements of the polarized components of the scattered signal supplemented with the data of contact measurements of the profile $\varepsilon[L]$. It should be noted that the polarized components can be measured only in a limited depth range because of the fast decrease caused by signal depolarization due to multiple scattering.

3. Methods based on inelastic interaction of laser radiation with matter

The considered group of methods is based on analysis of Raman spectra, fluorescence spectra, spectra of stimulated Brillouin and others excited by laser pulses in the UV and visible spectral regions.[1,5,18,20] The physical processes listed above are called inelastic interactions of radiation with the matter, in which the energy of a re-emitted quantum differs from the energy of the incident quantum.[1,18,19]

Raman scattering takes place for all chemical elements and compounds present in the irradiated volume of the sea water.[1,18,19] The main advantages of the method employing this effect are:

fixed shift of partial spectral components for admixtures with respect to the sensing signal;

proportionality of the intensity of partial spectral components to the concentration of admixtures;

limited duration of the Raman process allowing improvement of the signal/background ratio due to time gating;

possibility of obtaining panoramic spectra with a single laser.

A very valuable property is the dependence of the Raman scattering signal on the concentration of water molecules (which is constant). This allows the envelope of the Raman signal to be used as a reference for normalization of signals (Mie scattering, fluorescence) or (at spectral measurements) the Raman spectral line of water to be used for normalization of other spectral components.[5,20] In this case, the influence of destabilizing factors decreases significantly. The most important, among the destabilizing factors, is the roughness of the sea surface, the sensing and backscattering signals pass through.

However, the cross section of the Raman scattering is more than three orders of magnitude less than the cross section of Rayleigh scattering. This limits the capabilities of the method at remote sensing of the upper ocean layer.

Fluorescence is observed, when the laser radiation at the frequency of a certain electronic transition in an atom or molecule is absorbed with re-emission at a lower frequency.[19] In molecules, because of the presence of a group of energy levels, the radiation is broadband and the signal-to-noise ratio is low. Therefore, to employ the fluorescence effects, the time characteristics of the process are used as well.[1,19]

The intensity of fluorescence signals from organic compounds most abundant in the sea water at typical values of their concentrations is comparable with the Raman signal. Thus, to describe fluorescence properties of the sea water, we can introduce, similarly to the primary hydrooptical characteristics, the fluorescence parameter

$$\Phi_0 = I_{\mathrm{fl}}/I_{\mathrm{RS}}, \qquad (12)$$

where I_{fl} and I_{RS} are integral numbers of quanta in the measurement band.

This parameter is widely used when studying three main classes of organic compounds present in the sea water, namely, phytoplankton, dissolved organic matter (DOM), and oil products (OP).[20,42,43] Determining Φ_0 in the process of laser sensing, we solve the problem of mapping fluorescent fields and estimating their space-time variability. Comparison of data for different regions of water areas under study allows revealing pollution zones with the allowance for *a priori*

information on hydrological, hydrobiological, and hydrochemical characteristics of the area under study.

Atomic or resonance fluorescence is observed at the frequency of a certain transition in an atom that coincides with the frequency of sounding radiation. The cross section of this process is of the same order as that of the Rayleigh scattering, but collisions of quanta with molecules of prevailing substances lead to a fast decay of the process, or quenching.[19]

Stimulated Brillouin scattering is observed as laser radiation is scattered by condensed media due to interaction with natural elastic oscillations of these media (sonic or hypersonic waves); this effect is accompanied by the change of a set of frequencies characterizing the radiation.[18]

4. Lidar diagnostics of pollution of the marine environment by organic compounds (dissolved organic matter, oil products, phytoplankton)

Organic compounds polluting the marine environment can be divided into three main groups: dissolved organic matter (DOM), oil products (OP), some species of chlorophyll and phytoplankton, whose increased concentration is a consequence of anomalously intense growth in the presence of the primary polluting DOM.[49] For diagnostics of these pollutants, the methods of fluorimetry are usually used.

4.1. Peculiarities of diagnostics of dissolved organic matter

Complication of DOM diagnostics is caused by a number of factors. First, a very wide variety of compounds is present in the sea water, and the major part of them is still to be identified. Second, fluorescence spectra determined by a complex structure of organic molecules are strongly variable. Third, DOM spectra often overlap with OP spectra thus complicating their separation and assignment.

Note that some organic compounds have no absorption bands in the visible spectrum; therefore they cannot be detected by direct laser methods. The characteristics of DOM fluorescence have received much attention.[17,44–48]

For identification of compounds, the following characteristics can be used:

– wavelength of a fluorescence peak at a fixed excitation wavelength[19];

– shape of a fluorescence band, which can be described quantitatively as an intensity ratio at two wavelengths[44];

– fluorescence lifetime, which is independent of the wavelength and varies widely (0.1–100 ns) for different compounds[45];

– fluorescence saturation due to the change in the spectrum under the exposure to high-power laser radiation.[46,48]

4.2. Capabilities of diagnostics of pollution of the marine environment with oil products

Oil products in the sea water are subject to a number of physical and chemical processes resulting in formation of dissolved, emulsified, and dispersed fractions in the surface layer.[11,49,50] The fluorescence signal of the marine environment in this case is characterized by higher intensity as compared to the sea water with the background content of chlorophyll and DOM. In this case the Raman line of water is suppressed.[43,46,48,51]

Development of quantitative methods for OP detection is difficult because of their variety and transformation in the sea water. In Ref. 43 the method based on separated determination of the dissolved and emulsified fractions has been proposed. The properties inherent in every fraction proved to be close for all types of OP studied. Thanks to this fact, the algorithm has been developed for determination of the coefficient α in the relation between the concentration and the fluorescence parameter ($c = \alpha\Phi$). On this basis, the technique has been proposed for remote quantitative determination (without identification) of dissolved and emulsified fractions at different stages of OP aging.

4.3. Peculiarities in diagnostics of phytoplankton

Phytoplankton, as any other biological system, is very sensitive to the change of external conditions, in particular, to anthropogenic pollution, whose effect manifests itself[52–54]:

– in the change of the structure or in distortion of the size of populations producing phytoplankton up to complete disappearance of some species;

– in functional disorders of all phytoplankton forms at synthesis of a new organic substance and its decomposition in the process of intracellular destruction;

– in the toxic effect most pronounced in the period of active growth of algae at optimal temperature, illumination, and sufficient supply with biogenic elements.

The information on composition and properties of phytoplankton is in spectral and temporal characteristics of the fluorescence signals. A peculiarity of phytoplankton is the dependence of induced fluorescence signals (both time and intensity dependence, and in some cases spectral one) on the level of exciting radiation. The fluorescence characteristics are determined by phytoplankton pigments, which are conditionally subdivided into the following main groups[52,53,55,59]: chlorophylls (A, B, and C types), phycobilins, carotinoids, and xanthophylls.

The studies revealed that chlorophyll A is present in all types of algae for sea phytoplankton. The presence of phycobilins is characteristic of all types of cyanobacteria. So, it can serve as an indirect sign of pollution.

Ocean and, in most cases, sea chlorophyll has a rather narrow fluorescence band due to chlorophyll A. At excitation in the spectral region of 480–630 nm, the reference component of the Raman spectrum of water is situated optimally with respect to the fluorescence band of phytoplankton. When measuring the parameter Φ_0, its values can be referred to the concentration of chlorophyll A, value of biomass, or number of cells. There are standard techniques for determining these parameters.

Specific identification of the components of phytoplankton with the use of multifrequency laser fluorimetry is possible due to specific differences in the spectra.[56] Having knowledge on the dependences $\Phi_0(\lambda_{exc})$ for different components, one can identify them and determine their partial contributions to the total fluorescence band.[59] Recently, a number of methods have been proposed for diagnostics of DOM and OP; these methods improve the characteristics of traditional methods of fluorimetry.

4.4. Main methods for laser diagnostics of DOM, OP, and phytoplankton

The methods that are being intensely developed for diagnostics of organic pollutants in water by remote laser spectrometry are mostly aimed at identification of pollutants and estimation of their concentration regardless of what group (DOM, OP, or phytoplankton) they belong to. The above brief information on the state of the problem of DOM, OP, and phytoplankton diagnostics is indicative of its complexity because of extremely wide variety of components with overlapping spectra and different kinetics of spectra under the effect of numerous factors (geographic, climatic, meteorological, hydrophysical, hydrochemical, temporal, etc.). Thus, some methods of laser diagnostics can be used that employ particular informative indices of spectra due to rather fine physical effects.

These methods have been approved in field and laboratory experiments.[20,42,43,46–48,51,54–59]

Method of nonlinear fluorimetry is based on the fact that the nonlinearity coefficient is different for DOM and OP[47]:

$$\beta = \lim_{F \to 0} \frac{\partial \Gamma(F)}{\partial F}, \qquad (13)$$

where $\Gamma(F) = \Phi_0 / \Phi(F)$ and F is the density of photon flux.

However, this method is applicable only in the case of a single admixture present in the water.

Method of multifrequency fluorimetry[47] for separation of partial contributions of DOM and OP is based on the fact that the fluorescence parameter Φ_0 is different for different wavelengths of the exciting radiation. Measuring the resulting parameter $\Phi_0^{\Sigma} = \Phi_0^{DOM} + \Phi_0^{OP}$ at the wavelengths λ_1 and λ_2, we can determine the terms separately.

Method of TLS (Total Luminescence Spectra) diagrams[57] is based on recording fluorescence spectra under excitation at different wavelengths and plotting diagrams of equal radiation intensity for the cases of multicomponent admixtures.

Method of three-dimensional matrices,[58] i.e., a set of instantaneous spectra uses both spectral and temporal information on pollutants. This method belongs to kinetic spectroscopy with high temporal resolution (about 0.1 ns).

The methods of multifrequency fluorimetry and TLS diagrams can be considered as versatile relative to the main groups of organic pollutants.

Multispectral method[59] assumes the use of a tunable laser and may prove to be efficient because of the pronounced spectral selectivity of the absorption coefficient of chlorophyll pigments and its difference from the spectral dependences of the DOM scattering and absorption coefficients. The method is based on generation of a synthesized signal with the help of the difference algorithm $I_{dif} = B_{i1} - B_{i2}$, where B_{i1} and B_{i2} are the signals recorded in the corresponding spectral channels.

The application of the difference algorithm decreases the effect of additive noise arising as the incident radiation is reflected or scattered by an atmospheric layer, sea surface, and water layer above a recorded deep anomaly of chlorophyll-containing suspensions of stimulated bioluminescents.

4.5. Experimental results

In spite of the variety of the above-listed methods for diagnostics of organic compounds, the practice of remote laser sensing taking into account the state-of-the-art of the existing technical tools restricts itself, as a rule, to measurements of the fluorescence parameter and concentration of some chlorophyll species. Below we give some data of research conducted in the Black and Baltic Seas.

Reference 55 presents the experimental results on DOM in the Russian near-shore zone of the Black Sea. Both DOM and OP contributed to the fluorescence band. Therefore, when analyzing the results, we can speak only about estimation of the integral fluorescence parameter at the wavelength of 335 nm. The results of mapping of this parameter are shown in Fig. 5. The analysis shows that its value was below 0.1 in the most part of the studied water area. This is indicative of the low level of organic matter in the near-shore zone. An exception is a local spot, in which this parameter was 0.3.

The content of organic matter increased in the near-shore zone of towns (Tuapse, Lazarevskoe). Near a mouth of the Shepsi River, the content of the organic substance increased due to the influence of river run-off.

The distribution of the parameter Φ_0 drawn for a vast region of the Baltic Sea based on the results of monitoring[42] is shown in Fig. 6. One can see the influence of discharges of water with the increased content of organic matter in regions with intense industrial activity.

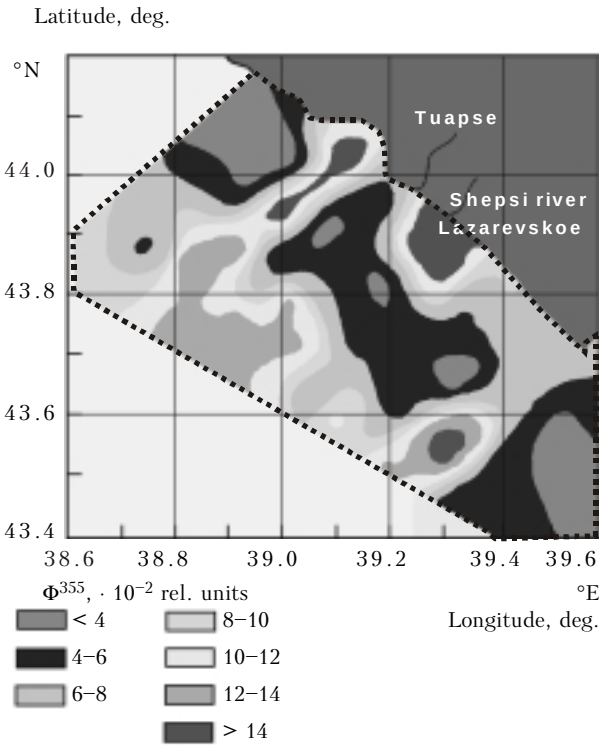

Fig. 5. Horizontal distribution of the fluorescence parameter Φ^{355} over the studied territory of the Black Sea.

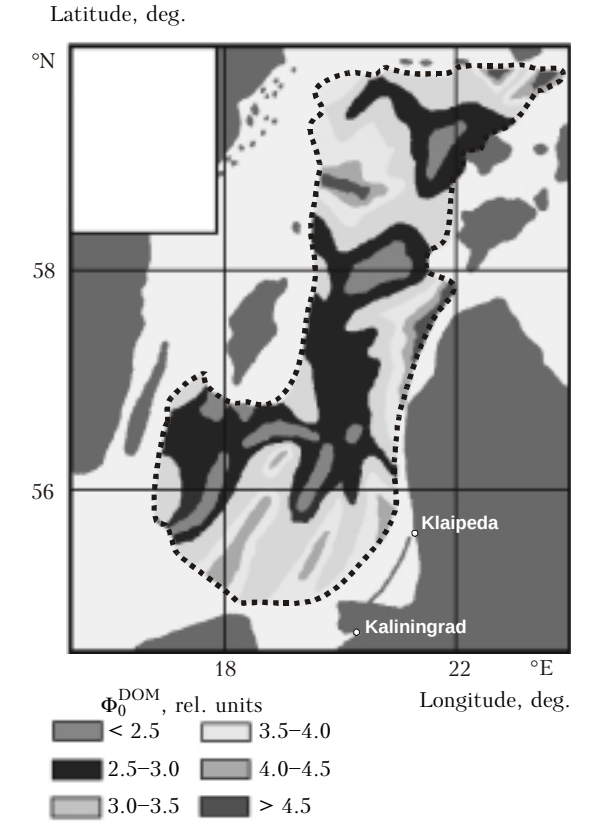

Fig. 6. Distribution of DOM fluorescence intensity in the surface layer of the Baltic Sea in May–June 1984.

5. Methods of lidar measurement of temperature and salinity of sea water

Temperature measurements by remote laser sensing are based on the effects of Raman scattering. The physical principles of the method are as follows[60]:

liquid water exists in at least two main forms: monomeric and polymeric (the polymeric form is characterized by additional bonds of hydroxyl groups between molecules); both forms are in equilibrium as functions of temperature;

broadening of the Raman spectral line of a hydroxyl group (O–H) differs markedly for the monomeric and polymeric forms;

intensities of the partial spectral components, corresponding to the monomeric λ_1 and polymeric λ_2 forms are proportional to their concentrations; thus, the equilibrium temperature can be determined from the intensity ratio of the components.

Since the cross section of Raman scattering is almost three orders of magnitude lower than the cross section of Rayleigh scattering, the depth range in temperature measurements is limited.[6] The accuracy of measurements is affected by such factors as sea roughness, noise of natural light field, induced laser fluorescence, and different propagation conditions for the two spectral components.

The known results have been obtained in shipborne measurements[60] and in measurements conducted from an offshore bench.[61] The maximum depth of measurements was ≤ 30 m. The error of temperature measurements did not exceed ±1°C.

Polarization method for temperature measurement uses the polarized sounding radiation. In this method, two Raman spectra of signals with orthogonal polarization are recorded. The ratio of the components is a function of wavelength and, in its turn, dependent on temperature. The estimates[60] show that the expected error is 0.5°C for the optical path length $\tau = \varepsilon L \leq 4$ at 1 J of emitted energy.

Methods of coherent anti-Stokes Raman scattering (CARS) belong to the methods of nonlinear laser spectroscopy.[23,24] These methods have some advantages in spectral and spatial resolution, signal-to-noise ratio, etc. However, they are still limited to laboratory experiments, because the necessary condition of their application is synchronism of interacting waves, but in remote sensing the pump source and the receiver are separated by the boundary of the medium under study. In Refs. 23 and 24, a modification of the polarization CARS method has been proposed and implemented under laboratory conditions. This modification principally suits remote measurements. In it, the pump wave is excited in a medium due to the process of stimulated backscattering (in particular, SBS). Analysis of laboratory experiments shows that the expected error of temperature measurements does not exceed ±1°C at the signal variance of 10%. Suppression of fluctuations down to 1% along with analysis of temperature changes

of other spectral parameters (line shape and width, etc.) will improve the measurement accuracy by more than an order of magnitude.

Method of envelope of Raman spectrum. The envelope of the Raman spectrum of the sea water depends not only on the temperature T, but also on the content of dissolved salt S. These parameters are estimated by measuring the intensity of components in different spectral channels according to the method from Ref. 62 on the assumption that the intensity of the Raman spectrum is a sum of linear functions

$$\xi_i = \alpha_{iT}T + \alpha_{iS}S + \beta_i + \nu_i, \qquad (14)$$

where i is the number of a spectral channel; α_{iT} and α_{iS} are the coefficients determining the effect of T and S on the Raman intensity in the ith channel; β_i is the constant equal to the mean Raman intensity in the ith channel at zero values of T and S; ν_i is a random error of measurement in the ith channel (with zero mean $E\nu_i = 0$ and known variance $E\nu_i^2 = \sigma_i^2$).

With the available set of measurements $\{\xi_i\}$ in i spectral channels, the problem of determination of T and S as random parameters with given statistical errors is formulated from the viewpoint of minimization of measurement errors on the average. To solve this problem, the parameters α_{iT} and α_{iS} should be known. These parameters are pre-determined in m test Raman spectra with known T and S. Test spectra are recorded at strictly dosed values of salinity of test solutions and monitored temperature.

To solve the problem on determination of T and S, the algorithm based on application of the mathematical apparatus of estimation theory has been proposed.[62] A simpler way to estimate T and S is to use the least-squares method.

According to the data of laboratory experiments, the measurement errors are the following: $\Delta T = \pm 0.7$°C and $\Delta S = \pm 1.05\lambda$.

6. Method for determining the content of heavy metals in marine environment (laser-spark method)

The idea of the laser-spark method is in initiation of a plasma formation on the sea surface under the exposure to a focused laser beam with high energy density of pulsed radiation and the following analysis of the spectrum of plasma glow in order to determine characteristic lines of atomic fluorescence of various elements.[63–66] The presence of free high-temperature electrons in plasma leads to excitation of atoms and molecules due to inelastic collisions in vapor. This causes its intense glow. The energy of lines in the emission spectrum at optical breakdown is several orders of magnitude higher than that of thermal glow of high-temperature vapor at laser radiation intensity lower than the optical breakdown threshold.

If in the Raman spectra only a 10^{-9}th part of the light flux participates in formation of the backscattering signal, then in a spark analyzer in the breakdown plasma up to 90% of laser pulse energy is actually absorbed. However, the pollutants that are sought have low concentrations in the presence of basic atmospheric constituents, namely, nitrogen and oxygen, whose concentration and, consequently, spectral line intensity is several orders of magnitude higher.

Nevertheless, this difficulty is overcome due to time selection of emission spectra. The dynamics of laser breakdown is such that the breakdown itself and heating of plasma occur during a laser pulse (10 to 100 ns in the proposed version of a lidar). As this takes place, the instantaneous electron temperature can achieve tens thousand degrees. After completion of the laser pulse, plasma expands (spreads) and cools down. In the course of this process, electrons with high ionization potential first leave the excited state. On the other hand, the cooling rate of the plasma decreases exponentially with time. Thus, due to time gating, the spectral lines of the basic atmospheric constituents can be made many orders of magnitude weaker. This is a qualitative description of the process, because its physical-mathematical model determined by numerous factors is extremely complex and is not still at the level of accurate quantitative equations for description of the spectral parameters of the pollutants to be detected.

Under field conditions, the method of laser spark emission analysis can be used with a lidar supplemented with a multichannel spectrometer and a unit for beam focusing. The laser-emission analysis does not impose any particular requirements on the radiation wavelength.

The proposed version of a helicopter-borne lidar system[6,65] employs a solid-state Nd^{3+}YAG laser operated in the frequency doubling mode. The basic parameters of the lidar system are the same as in the case of sensing water.

The marine medium can be analyzed for the presence of heavy metals (Cu, Pb, Hg, Cd, Co, etc.) and their compounds, as well as other dangerous pollutants from the height of 10–15 m.

The minimum detectable concentrations of the analyzed pollutants are about 10^{-2}–10^{-3}%. Under laboratory conditions these values can be as low as 10^{-7}%. The spectral resolution of the system is 1.1 nm/channel. The sensitivity in the region of 200–800 nm is about 1000 phot./reading.

For assignment of spectral lines, the database has been compiled for atomic-fluorescent analysis. This database includes about 80 000 lines for 60 most abundant elements.[65]

Conclusion

Analysis of lidar methods presented shows their efficiency as applied to remote diagnostics of pollution of the marine environment. These methods can be used for studying such characteristics as turbidity, salinity,

and temperature, as well as for detecting DOM, dissolved, emulsified, and dispersed OP, dissolved oxygen, nitrogen, phosphorus, heavy metals, and others in the sea water. The study of the turbidity field and statistical characteristics of sea roughness can provide information on hydrodynamic processes occurring in the sea depth, and this information can be used for detection of anthropogenic pollution and for mapping of a polluted region.

The laser remote sensing methods can be useful in determining the concentration of main components of phytoplankton and other biogenic components. These data constitute a part of information on the ecological state of water. When using the developed specialized models of sea shelf ecosystems, this information allows evaluation of the risk for living components of ecosystems and determination of the permissible anthropogenic load on a shelf water area.[8,12,67]

The following lidar methods are best developed now: method for estimating the variability of the turbidity field based on analysis of the envelope of the backscattering signal, method of laser fluorimetry with normalization to the Raman signal for determining the DOM, OP, and phytoplankton concentrations, and the method of temperature measurement based on Raman scattering.

Under nowadays conditions, when funding for experiments with airborne lidars is limited, it is especially important to improve the methods for processing and analysis of the data accumulated earlier. Works in this field can form a basis for the development of new methods of lidar diagnostics, whose range of application to the study of the World Ocean will be much wider than that discussed in this paper.

References

1. R.M. Measures, *Laser Remote Sensing* (Wiley, New York, 1987).
2. V.E. Zuev, ed., *Laser Sensing of the Atmosphere and Underlying Surface* (Nauka, Novosibirsk, 1991), 147 pp.
3. V.E. Zuev, *Propagation of Laser Radiation in the Atmosphere* (Radio i Svyaz', Moscow, 1981), 286 pp.
4. M.V. Kabanov, ed., *Remote Monitoring of the Upper Ocean Layer* (Nauka, Novosibirsk, 1987), 262 pp.
5. A.F. Bunkin, D.V. Vlasov, and D.M. Mirkamilov, *Physical Principles of Laser Sensing of the Earth's Surface* (FAN, Tashkent, 1987), 272 pp.
6. F.V. Bunkin and A.F. Bunkin, Atmos. Oceanic Opt. **13**, No. 1, 54–60 (2000).
7. R.F. Lutomirski, SPIE **2222**, 12–19.
8. V.G. Bondur, in: *Aerospace Information Systems.* Vol. 2. *Scientific Principles of Creation and Application of Aerospace Systems for Earth Observation*, ed. by V.G. Bondur and A.I. Savin (Nauka, Moscow, 2000), 496 pp.
9. V.G. Bondur, in: *Proceedings of Global Environmental Disaster Monitoring Subgroup of the Environmental Workgroup of the Gore–Chernomyrdin Russian–American Commission on Economic and Technological Cooperation* (Ministry of Environmental Protection and Natural Resources of the Russian Federation, Moscow, 1996), 26 pp.
10. V.G. Bondur, in: *Gore–Chernomyrdin Environmental Working Group. Initiative Proceeding of the Global Environmental Disaster Monitoring Subgroup Meeting* (Rosslin, Virginia, USA, 1996), 24 pp.
11. Yu.A. Izrael' and A.V. Tsyban', *Anthropogenic Ecology of Ocean* (Gidrometeoizdat, Leningrad, 1989), 528 pp.
12. A.I. Savin and V.G. Bondur, Atmos. Oceanic Opt. **13**, No. 1, 38–53 (2000).
13. V.G. Bondur, Izv. Vyssh. Uchebn. Zaved., Ser. Geodeziya i Aerofotos'emka, Nos. 1–2, 14–27 (1995).
14. *Ocean Optics.* Vol. 1. *Physical Optics of Ocean.* Vol. 2. *Applied Ocean Optics* (Nauka, Moscow, 1983), 371 pp., 236 pp.
15. A.P. Ivanov, *Physical Principles of Hydrooptics* (Vysshaya Shkola, Minsk, 1976), 504 pp.
16. H. Walter, ed., *Laser Spectroscopy of Atoms and Molecules* (Springer-Verlag, Berlin-Heidelberg, New-York, 1976).
17. F. Lakovich, *Principles of Fluorescent Spectroscopy* [Russian Translation] (Mir, Moscow, 1986), 496 pp.
18. I.L. Fabelinskii, *Molecular Scattering of Light* (Moscow, 1965).
19. G.S. Landsberg, *Optics* (Nauka, Moscow, 1976), 926 pp.
20. D.N. Klyshko and V.V. Fadeev, Dokl. Akad. Nauk SSSR **238**, No. 2, 320 (1978).
21. L.S. Dolin and I.M. Levin, *Handbook on Theory of Underwater Vision* (Gidrometeoizdat, Leningrad, 1991), 229 pp.
22. R.N. Keeler and B.L. Ulich, SPIE **2258** *Ocean Optics XII*, 480–501.
23. A.F. Bunkin, D.V. Vlasov, and R.A. Garaev, Kvant. Elektron. **10**, 669–671 (1983).
24. A.F. Bunkin, D.V. Vlasov, and R.A. Garaev, Kvant. Elektron. **10**, 1902–1903 (1983).
25. Bin Zheng, C.M. Pleass, and C.C. Ih, Appl. Opt. **33**, No. 2, 231–237 (1994).
26. A. Ivanov, *Introduction to Oceanography* [Russian Translation] (Mir, Moscow, 1978), 574 pp.
27. J.D. Klett, Appl. Opt. **20**, No. 27, 211–220 (1981).
28. M. Kaestner, Wiss. Mitt. Meteorol. Inst. Munchen, No. 56, 148–156 (1987).
29. B. Billard, R.H. Abbot, and M.F. Penny, Appl. Opt. **25**, No. 13, 2080–2088 (1986).
30. L.S. Dolin and V.A. Savel'ev, in: *Sea Optics* (Nauka, Moscow, 1983), pp. 123–128.
31. D.V. Vlasov, E.V. Zubkov, and S.I. Shamaev, Atmos. Oceanic Opt. **8**, No. 9, 706–710 (1995).
32. F.V. Bunkin, D.V. Vlasov, E.V. Zubkov, et al., in: *Abstracts of Reports at Interbranch Scientific Technical Meeting on Statistical Methods and Systems for Processing of Remote Sensing Data,* Sevchenko Institute of Applied Physical Problems, Minsk, (1989), pp. 149–151.
33. E.V. Zubkov and A.F. Bunkin, Bulletin of Russian Academy of Sciences (BRAS)/ Supplements Physics of Vibrations **59**, No. 3, 165–172 (1995).
34. I.E. Penner and V.S. Shamanaev, Opt. Atm. **1**, No. 2, 92–96 (1988).
35. O.A. Bukin, V.I. Il'ichev, I.A. Kritskii, and A.N. Pavlov, "*Some results of lidar sensing of the upper ocean layer,*" Preprint of Pacific Oceanological Institute of the Far East Branch of the Academy of Sciences of the USSR (Vladivostok, 1989), 6 pp.
36. O.A. Bukin, V.D. Kiselev, S.A. Klenin, et al., "*Complex photoacoustic sensing of the upper ocean layer,*" Preprint of Pacific Oceanological Institute of the Far East Branch of the Academy of Sciences of the USSR (Vladivostok, 1988), 18 pp.

37. F.E. Hoge, C.W. Wright, et al., Appl. Opt. **27**, No. 19, 3969–3977 (1988).
38. A.P. Vasilkov, T.V. Kondranin, and E.V. Myasnikov, Izv. Akad. Nauk SSSR, Ser. Fiz. Atmos. Okeana **26**, No. 3, 307–312 (1990).
39. A.P. Vasilkov, T.V. Kondranin, and E.V. Myasnikov, in: *Proceedings of PORSEC*, Okinava (1992), Vol. 2, pp. 1058–1062.
40. A.P. Vasilkov, Y.A. Goldin, and B.A. Gureyev, SPIE **1936**, *Appl. Laser Radar Technology,* 233–244 (1993).
41. A.I. Abramochkin, I.I. Zanin, and I.E. Penner, Opt. Atm. **1**, No. 2, 92–96 (1988).
42. A.A. Demidov, A.M. Chekalyuk, T.V. Lapshenkova, and V.V. Fadeev, Meteorol. Gidrol., No. 6, 62–70 (1988).
43. A.G. Abroskin, S.E. Nol'de, V.V. Fadeev, and V.V. Chubarov, Dokl. Akad. Nauk SSSR (1987).
44. J.F. Fantasia and H.C. Ingrao, in: *Proc. of Joint Conf. on Prevention Control of Oil Spills*, Washington, USA (1973), pp. 101–115.
45. D.M. Rayner and A.G. Szabo, Appl. Opt. **17**, No. 10, 16–24 (1978).
46. V.V. Fadeev, A.M. Chekalyuk, and V.V. Chubarov, Dokl. Akad. Nauk SSSR **262**, No. 2, 338–341 (1982).
47. A.G. Abroskin, S.E. Nol'de, V.V. Fadeev, et al., in: *Proc. of 12th All-Union Conference on Coherent and Nonlinear Optics*, Moscow (1985), Part II, p. 560.
48. T.A. Alekseeva and T.A. Teplitskaya, *Spectrofluorimetric Methods for Analysis of Aromatic Hydrocarbons in Natural and Technological Media* (Gidrometeoizdat, Leningrad, 1981), 215 pp.
49. *Problems of Chemical Pollution of World Ocean.* Vols. 1–9 (Gidrometeoizdat, Leningrad, 1985).
50. A.M. Vladimirov, Yu.I. Lyakhov, L.T. Matveev, and V.G. Orlov, *Environmental Protection* (Gidrometeoizdat, Leningrad, 1991), 424 pp.
51. S.V. Lyutsarev and V.V. Chubarov, Atmos. Oceanic Opt. **7**, No. 4, 254–259 (1994).
52. M.E. Vinogradov, ed., *Oceanology. Ocean Biology.* Vol. 1. *Biological Structure of Ocean* (Nauka, Moscow, 1977), 427 pp.
53. M.E. Vinogradova, in: *Global Ecological Problems on the Verge of XXI Century* (Nauka, Moscow, 1998), pp. 99–148.
54. S.A. Patin, in: *Oceanology. Ocean Biology.* Vol. 2B. *Biological Productivity of Ocean,* ed. by. A.S. Monin (Nauka, Moscow, 1977), pp. 322–331.
55. D.K. Bunin, M.Yu. Gorbunov, et al., Izv. Ros. Akad. Nauk, Ser. Fiz. Atmos. Okeana **29**, No. 1, 131–139 (1993).
56. P.B. Mutola, J. Jaretto, and C.A. Brown, in: *II Joint Conf. on Sensing of Environmental Pollutants*, Washington (1973), p. 53.
57. A.E. Dudelzak, S.M. Babichenko, and L.V. Poryvkina, Appl. Opt. **30**, No. 4, 453–457 (1991).
58. F.J. Knorr and J.M. Harris, Anal. Chem. **53**, No. 2, 272–276 (1981).
59. V.V. Fadeev, Kvant. Elektron. **5**, No. 10, 2221 (1978).
60. D.A. Leonard, B. Caputo, and F.E. Hoge, Appl. Opt. **18**, No. 11, 1732–1745 (1979).
61. *Scientific Technical Report* (Institute of General Physics AS USSR, Moscow, 1983).
62. P.V. Golubtsov, T.A. Gogolinskaya, E.M. Kim, et al., Morskoi Gidrofiz. Zh., No. 1, 59–64 (1988).
63. A.M. Prokhorov, D.V. Vlasov, D.Yu. Tsipenyuk, and V.S. Bukreev, Zh. Prikl. Spektrosk. **55**, No. 2, 313–314 (1991).
64. D.V. Vlasov, A.M. Prokhorov, D.Yu. Tsipenyuk, and V.S. Bukreev, Atm. Opt. **4**, No. 4, 337–338 (1991).
65. A.F. Bunkin, A.V. Rezov, and D.Yu. Tsipenyuk, Zh. Teor. Fiz. **64**, No. 3, 195–200 (1994).
66. O.A. Bukin, Yu.A. Zanin, E.A. Sviridenkov, et al., Atmos. Oceanic Opt. **5**, No. 11, 780–782 (1992).
67. V.I. Belyaev and N.V. Konduforova, *Mathematical Simulation of Ecological Shelf Systems* (Naukova Dumka, Kiev, 1990), 242 pp.